

Noise amplification in frictional systems: Oscillatory instabilities

Joyjit Chattoraj,¹ Oleg Gendelman,² Massimo Pica Ciamarra,^{1,3,*} and Itamar Procaccia⁴

¹*School of Physical and Mathematical Sciences, Nanyang Technological University, 637371 Singapore*

²*Faculty of Mechanical Engineering, Technion, Haifa 32000, Israel*

³*CNR–SPIN, Dipartimento di Scienze Fisiche, Università di Napoli Federico II, I-80126, Napoli, Italy*

⁴*Department of Chemical Physics, The Weizmann Institute of Science, Rehovot 76100, Israel*



(Received 25 March 2019; published 3 October 2019)

It was discovered recently that frictional granular materials can exhibit an important mechanism for instabilities, i.e., the appearance of pairs of complex eigenvalues in their stability matrix. The consequence is an oscillatory exponential growth of small perturbations which are tamed by dynamical nonlinearities. The amplification can be giant, many orders of magnitude, and it ends with a catastrophic system-spanning plastic event. Here we follow up on this discovery, explore the scaling laws characterizing the onset of the instability, the scenarios of the development of the instability with and without damping, and the nature of the eventual system-spanning events. The possible relevance to earthquake physics and to the transition from static to dynamic friction is discussed.

DOI: [10.1103/PhysRevE.100.042901](https://doi.org/10.1103/PhysRevE.100.042901)

I. INTRODUCTION

Understanding how granular materials fail is a problem of great geophysical importance due to its relevance to common phenomena like earthquakes and landslides. From a theoretical viewpoint, a micromechanical description of the failure process is difficult due to the absence of a Hamiltonian description of granular systems. To stress the importance of this, recall that starting from the pioneering works of Malandro and Lacks [1,2], plastic failures in athermal amorphous systems (with forces derivable from a Hamiltonian) have been identified as resulting from saddle node bifurcations occurring as a minimum of the energy landscape becomes a saddle point as the system deforms. In this approach, one considers a system of N particles whose center of mass coordinates are $\mathbf{r}_1, \mathbf{r}_2, \dots, \mathbf{r}_N$ at temperature $T = 0$ which is endowed with a Hamiltonian $U(\mathbf{r}_1, \mathbf{r}_2, \dots, \mathbf{r}_N)$. The dynamics of the system is written as Newton's equations of motion:

$$m_i \frac{d^2 \mathbf{r}_i}{dt^2} = \mathbf{F}_i(\mathbf{r}_1, \mathbf{r}_2, \dots, \mathbf{r}_N) \equiv - \frac{\partial U(\mathbf{r}_1, \mathbf{r}_2, \dots, \mathbf{r}_N)}{\partial \mathbf{r}_i}. \quad (1)$$

When the system is in mechanical equilibrium, the force \mathbf{F}_i on each particle vanishes,

$$\mathbf{F}_i \equiv - \frac{\partial U(\mathbf{r}_1, \mathbf{r}_2, \dots, \mathbf{r}_N)}{\partial \mathbf{r}_i} = 0 \quad \text{in equilibrium}. \quad (2)$$

The stability against perturbations of the equilibrium state is determined by the second derivative of the Hamiltonian, which is the Hessian matrix:

$$H_{ij}^{\alpha\beta} \equiv \frac{\partial F_i^\alpha}{\partial r_j^\beta} \equiv - \frac{\partial^2 U(\mathbf{r}_1, \mathbf{r}_2, \dots, \mathbf{r}_N)}{\partial r_i^\alpha \partial r_j^\beta}. \quad (3)$$

The Hessian matrix is evidently real and symmetric, and it has real eigenvalues which are all positive as long as the material is mechanically stable. Subjected to mechanical strain or stress, the system may display a saddle node bifurcation with an eigenvalue going to zero. Generically this bifurcation results in the localization of the associated eigenfunction, in accordance with a local release of stress and energy [3]. The modes of the Hessian matrix which are associated with such instabilities are known as “plastic” or “soft” modes, and their probability density function differs from the usual Debye density of states in purely elastic materials [4,5]. Work was devoted to understand the system size dependence of the eigenvalues of the Hessian [5] and their role in determining the mechanical characteristics such as the elastic moduli [6], the failure of nonlinear elasticity in such materials [6–8], and their relevance to shear banding and mechanical failure [9–11].

The dynamics of granular systems is governed by interparticle interaction forces, which have both normal and tangential components, obtained by coarse graining the microscopic degrees of freedom of the particles. A variety of different models exist [12–17], reflecting the different assumptions made in the derivation of the effective forces. In all cases, these forces cannot be expressed as derivatives of a Hamiltonian function with respect to the coarse-grained degrees of freedom, which are the translational and the angular displacements of the particles. It is worth stressing that the lack of a Hamiltonian description is not exclusively related to the presence of viscous or hysteretic forces but rather is inherent in the coupling between the coarse-grained tangential and normal forces. This implies that granular materials lack a Hamiltonian description even when dissipative forces may play a negligible role. As a consequence, the micromechanics of the failure process of granular systems cannot be understood using Hessian methods. Hence the question arises: How do granular materials fail?

*massimo@ntu.edu.sg

Previous works investigating the loss of mechanical rigidity of granular assemblies have suggested that this could originate [18] from local events related to the discontinuity of the frictional interaction between macroscopic objects. Indeed, the magnitude $|\mathbf{F}_{ij}^{(t)}|$ of the tangential force acting between two macroscopic objects i and j is bounded by $\mu|\mathbf{F}_{ij}^{(n)}|$, where $\mathbf{F}_{ij}^{(n)}$ is the normal interaction force and μ is Coulomb's friction coefficient. Accordingly, contacts may reach their Coulomb threshold and start slipping as stress or strain is applied to a granular assembly. The failure of a contact could trigger subsequent rearrangements of other grains in an avalanche process [19,20] or lead to the emergence of a percolating cluster of unstable grains [21–23], hence inducing the macroscopic failure of the system. A complementary approach to rationalize the failure of granular systems has been devised building on the theory for the instability of elastic-plastic solids [24], describing failure as a sharp increase of the kinetic energy of the system. When a granular system is slowly deformed, work is done on the system. Failure might occur when the system becomes unstable, meaning that the work done on the system, and possibly other work done by the system, is converted into kinetic energy. This so-called second-order work failure criterion [25] is formalized at the level of continuum equations and is therefore not suitable to investigating the underlying microscopic features leading to the instability. Nevertheless, this criterion is indirectly related to the instability criterion developed for Hamiltonian systems and hints towards the existence of collective failure modes. Support for the existence of a collective failure mechanism not initiated by the Coulomb failure of a contact also comes from detailed numerical simulations of model frictional granular particles, subject to an increase in shear stress. These simulations have shown that a granular system may become unstable without any new contact reaching its Coulomb threshold [26]—only after the system becomes unstable and starts slipping are new contacts seen to reach their Coulomb limit. An indirect support towards the existence of collective failure mechanisms also stems from the existence of a linear regime in the response of granular systems to applied perturbations [27–31], which is not easily rationalized assuming failure to originate from an underlying discontinuous process such as the Coulomb failure of a contact.

In a recent article [32] we identified an instability mechanism in systems lacking a Hamiltonian description, such as frictional amorphous solids. This instability mechanism involves an oscillating exponential growth of deviations from the state of mechanical equilibrium, and it is not related to the existence of a Coulomb threshold. It cannot exist in amorphous solids in which the interparticle forces are derived from a Hamiltonian. These oscillatory instabilities furnish a micromechanical mechanism for a giant amplification of small perturbations that can lead to system-spanning plastic events and mechanical failure. This physics was demonstrated in the context of amorphous assemblies of frictional disks, but the mechanism is generic for systems with friction. In this paper we follow up and discuss the phenomenon in greater detail.

The structure of the paper is as follows: In Sec. II we explicitly show that the coarse-grained description of the interparticle interaction of granular systems is not

Hamiltonian and introduce a modified interaction model that, while not-Hamiltonian, is at least differentiable. In Sec. III we review the instability mechanism for frictional systems that we identified in Ref. [32] and then describe its critical features. Using the numerical model illustrated in Sec. IV, we test our theoretical predictions concerning the birth of the instability in Sec. V. We discuss the growth of the instability until nonlinear dynamics set in, culminating in a system-spanning catastrophic event in Sec. VI. Section VII provides information on the effect of damping. The upshot of the discussion is that a threshold damping frequency can be defined (based on the instability amplification frequency) below which the instability dynamics is unperturbed by damping. Section VIII raises the important issue of how generic is the instability discussed in this paper. Does its existence depend on the details of the coarse-grained model used, or do we expect it to appear generically in any models that employ a reduced set of coordinates like the positions of the centers of mass of the granules and their angular coordinates. We provide arguments for the generality of the phenomenon but propose that at this point in time experiments should be invoked as the final test. In Sec. IX we summarize the paper and discuss the possible connection of the present findings to remote triggering in earthquakes and to the transition from static to dynamic friction. The road ahead and future research are described.

II. NON-HAMILTONIAN DESCRIPTION OF GRANULAR SYSTEMS

Coarse-grained descriptions of frictional amorphous solids, in which the effective degrees of freedom are the translational and the angular positions of the particles, do not admit a Hamiltonian description. To explicitly show that this is the case, we recap here a popular and time-honored model used to describe the interaction between frictional granular particles, but the conclusion remains valid for other models.

The interaction between two particles, that we assume spherical for simplicity, has a normal and a tangential component. The normal force is determined by the overlap $\delta_{ij} \equiv \sigma_i + \sigma_j - r_{ij}$ between the particles, where $\mathbf{r}_{ij} \equiv \mathbf{r}_i - \mathbf{r}_j$ and σ_i is the radius of particle i , and it is given by the Hertzian model,

$$\mathbf{F}_{ij}^{(n)} = k_n \delta_{ij}^{3/2} \hat{\mathbf{r}}_{ij}, \quad \hat{\mathbf{r}}_{ij} \equiv \mathbf{r}_{ij}/r_{ij}. \quad (4)$$

The tangential force is a function of the tangential displacement \mathbf{t}_{ij} between the particles, a vector which is always orthogonal to $\hat{\mathbf{r}}_{ij}$. Upon first contact between the particles, $\mathbf{t}_{ij} = 0$. Providing every particle with the angular coordinate θ_i , the change in tangential displacement is given by

$$d\mathbf{t}_{ij} = d\mathbf{r}_{ij} - (d\mathbf{r}_{ij} \cdot \mathbf{r}_{ij})\hat{\mathbf{r}}_{ij} + \hat{\mathbf{r}}_{ij} \times (\sigma_i d\theta_i + \sigma_j d\theta_j). \quad (5)$$

Accordingly, \mathbf{t}_{ij} is obtained by integrating over time the relative velocity of the particles at the point of contact. In the Mindlin model, the tangential force depends on \mathbf{t}_{ij} and on the contact area, which is proportional to $\sqrt{\delta_{ij}}$ [12],

$$\mathbf{F}_{ij}^{(t)} = -k_t \delta_{ij}^{1/2} \mathbf{t}_{ij} \hat{\mathbf{t}}_{ij}, \quad (6)$$

and satisfies the Coulomb condition

$$\mathbf{F}_{ij}^{(t)} \leq \mu \mathbf{F}_{ij}^{(n)}, \quad (7)$$

where μ is the friction coefficient. Usually this law is interpreted such that the tangential force reaches the limit abruptly, not analytically, thus not allowing derivatives of the tangential force to be computed.

We can see now why the interaction is not Hamiltonian and the Hessian does not exist in this case. The first reason is somewhat trivial, stemming from the nonanalyticity of the Coulomb law. This can be easily taken care of by smoothing out the Coulomb law such that the tangential force will have smooth derivatives; we choose

$$\mathbf{F}_{ij}^{(t)} = -k_t \delta_{ij}^{1/2} \left[1 + \frac{t_{ij}}{t_{ij}^*} - \left(\frac{t_{ij}}{t_{ij}^*} \right)^2 \right] t_{ij} \hat{t}_{ij}, \quad (8)$$

$$t_{ij}^* \equiv \mu \frac{k_n}{k_t} \delta_{ij}.$$

Now the derivative of the force with respect to t_{ij} vanishes smoothly at $t_{ij} = t_{ij}^*$ and the Coulomb law Eq. (7) is fulfilled.

The second reason for the loss of the Hessian matrix is not trivial at all [33]. The time honored Hertz-Mindlin effective forces presented here, even for disks or balls, are not derivable from a potential, due to the coupling between the normal and the tangential displacement in the tangential force. Notice that this coupling is physical, as the tangential force depends on the normal force since it determines the contact area. This is the origin of the term $\delta_{ij}^{1/2}$ in Eqs. (6) and (8). It is easy to see that, because of this term, the derivative of the normal force with respect to t does not equal the derivative of the tangential force with respect to δ , which is what occurs when the forces are derived from a Hamiltonian $U(\delta, t)$.

III. OSCILLATORY INSTABILITIES: THEORY

A. Stability matrix

While granular materials are not Hamiltonian, their dynamics is still Newtonian, with an extended set of coordinates $\mathbf{q}_i = \{\mathbf{r}_i, \boldsymbol{\theta}_i\}$:

$$m_i \frac{d^2 \mathbf{r}_i}{dt^2} = \mathbf{F}_i(\mathbf{q}_1, \mathbf{q}_2, \dots, \mathbf{q}_N), \quad (9)$$

$$I_i \frac{d^2 \boldsymbol{\theta}_i}{dt^2} = \mathbf{T}_i(\mathbf{q}_1, \mathbf{q}_2, \dots, \mathbf{q}_N), \quad (10)$$

where m_i are masses for the center of mass coordinates, I_i are moments of inertia for the angles, and \mathbf{F}_i are forces and \mathbf{T}_i are torques, respectively. Using the smoothed-out force Eq. (8), this allows us to define the stability matrix, which is an operator obtained from the derivatives of the force \mathbf{F}_i and the torque \mathbf{T}_i on each particle with respect to the coordinates. In other words,

$$J_{ij}^{\alpha\xi} \equiv \frac{\partial \tilde{F}_i^\alpha}{\partial q_j^\xi}, \quad \tilde{\mathbf{F}}_i \equiv \sum_j \tilde{\mathbf{F}}_{ij}, \quad (11)$$

where \mathbf{q}_j stands for either a spatial position or a tangential coordinate, and $\tilde{\mathbf{F}}_i$ stands for either a force or a torque. Since in the usual case $\mathbf{F}_i = -\partial U / \partial \mathbf{r}_i$, we see that the operator \mathbf{J} is an analog of the Hessian, even when a Hamiltonian description is lacking, but with a huge difference: \mathbf{J} is not a symmetric operator. Being real, it can possess pairs of

complex eigenvalues. When these appear, the system will exhibit oscillatory instabilities, since one of each complex pair will cause an oscillatory exponential divergence of any perturbation and the other an oscillatory exponential decay. The actual calculation of the operator \mathbf{J} is somewhat cumbersome if conceptually straightforward. A detailed calculation for the present case of frictional disks interacting via Eqs. (4) and (8) is presented in Appendix.

B. The oscillatory instability

When a pair of complex eigenvalues $\lambda_{1,2} = \lambda_r \pm i\lambda_i$ is born, an instability mechanism develops. It should be stressed that the birth of a pair of complex eigenvalues is *not* a Hopf bifurcation [34]. A pair of complex conjugate eigenvalues correspond to FOUR solutions $e^{i\omega t}$ to the linearized equation of motion with

$$i\omega_{1,2} = \omega_i \pm i\omega_r, \quad i\omega_{3,4} = -\omega_i \pm i\omega_r, \quad (12)$$

with $\omega_r \pm i\omega_i = \sqrt{\lambda_r \pm i\lambda_i}$. The first pair in Eq. (12) will induce an oscillatory motion with an exponential growth of any deviation $\mathbf{q}(0)$ from a state of mechanical equilibrium:

$$\mathbf{q}(t) = \mathbf{q}(0) e^{\omega_i t} \sin(\omega_r t). \quad (13)$$

The second pair represents an exponentially decaying oscillatory solution. The actual spatial dynamics that sets in due to this instability will be discussed below in Sec. VIA.

C. Universal scaling laws

Noticing that the instability under discussion is somewhat unusual, we address the question of how the coalescence of two real eigenvalues and the bifurcation of two imaginary parts take place as a function of the imposed strain. As noticed above, we need at least four degrees of freedom to have this instability, which means either four first-order equations or two second-order equations. Since we are solving Newton's equations of motion we will discuss the instability in the latter form.

The bifurcation we are dealing with has codimension 1, as it is driven by the change of a single parameter [34]. We note this parameter as γ for obvious reasons. We therefore consider the pair of equations

$$\begin{aligned} \ddot{x}_1 + f_1(x_1, x_2, \gamma) &= 0, \\ \ddot{x}_2 + f_2(x_1, x_2, \gamma) &= 0. \end{aligned} \quad (14)$$

We assume that both functions f_1, f_2 are analytic with respect to all their arguments. Let us also assume that the system (14) has a family of equilibrium points $[\tilde{x}_1(\gamma), \tilde{x}_2(\gamma)]$ for some interval of γ , so that

$$\begin{aligned} f_1[\tilde{x}_1(\gamma), \tilde{x}_2(\gamma), \gamma] &= 0, \\ f_2[\tilde{x}_1(\gamma), \tilde{x}_2(\gamma), \gamma] &= 0, \quad \gamma \in (\gamma_1, \gamma_2). \end{aligned} \quad (15)$$

Next we define the new variables $y_1 = x_1 - \tilde{x}_1(\gamma)$, $y_2 = x_2 - \tilde{x}_2(\gamma)$. Then, system (14) is rewritten as follows:

$$\begin{aligned} \ddot{y}_1 + F_1(y_1, y_2, \gamma) &= 0, \\ \ddot{y}_2 + F_2(y_1, y_2, \gamma) &= 0, \\ F_k &= f_k[y_1 + \tilde{x}_1(\gamma), y_2 + \tilde{x}_2(\gamma), \gamma], \quad k = 1, 2. \end{aligned} \quad (16)$$

By construction, Eqs. (16) possesses equilibria $(y_1, y_2) = (0, 0)$ for $\gamma \in (\gamma_1, \gamma_2)$. Therefore, using analyticity, we rewrite Eqs. (16) as follows:

$$\begin{aligned} \ddot{y}_1 + c_{11}(\gamma)y_1 + c_{12}(\gamma)y_2 + O(|y_1|^2, |y_2|^2, |y_1y_2|) &= 0, \\ \ddot{y}_2 + c_{21}(\gamma)y_1 + c_{22}(\gamma)y_2 + O(|y_1|^2, |y_2|^2, |y_1y_2|) &= 0, \\ c_{kl}(\gamma) &= \left. \frac{\partial F_k(y_1, y_2, \gamma)}{\partial y_l} \right|_{(y_1, y_2)=(0,0)}. \end{aligned} \quad (17)$$

Removing the nonlinearities and taking $y_1 = y_1^{(0)} \exp(i\omega t)$, $y_2 = y_2^{(0)} \exp(i\omega t)$, one obtains the following equation for the eigenvalues:

$$[c_{11}(\gamma) - \lambda][c_{22}(\gamma) - \lambda] - c_{12}(\gamma)c_{21}(\mu) = 0, \quad \lambda = \omega^2. \quad (18)$$

The solution is obvious:

$$\begin{aligned} \lambda_{1,2} &= \frac{c_{11}(\gamma) + c_{22}(\gamma) \pm \sqrt{D(\gamma)}}{2}, \\ D(\gamma) &= [c_{11}(\gamma) - c_{22}(\gamma)]^2 + 4c_{12}(\gamma)c_{21}(\gamma). \end{aligned} \quad (19)$$

Finally, we identify the critical point where the real eigenvalues coincide as $\gamma = \gamma_c$, $\gamma_c \in (\gamma_1, \gamma_2)$. Then it must be that $D(\gamma_c) = 0$. In the vicinity of γ_c we assume generic dependence of all functions on the parameters and get the following:

$$\begin{aligned} \lambda_{1,2} &= \frac{c_{11}(\gamma_c) + c_{22}(\gamma_c) \pm \sqrt{\alpha(\gamma - \gamma_c)}}{2} + O(|\gamma - \gamma_c|), \\ \alpha &= D'(\gamma)|_{\gamma=\gamma_c}. \end{aligned} \quad (20)$$

Without loss of generality, we can assume $\alpha > 0$. Finally, for the eigenvalues near the bifurcation point we have

$$\begin{aligned} \lambda_1 - \lambda_2 &= \sqrt{\alpha(\gamma - \gamma_c)} + O(|\gamma - \gamma_c|), \quad \gamma > \gamma_c, \\ \Im(\lambda_1 - \lambda_2) &= \sqrt{\alpha|\gamma - \gamma_c|} + O(|\gamma - \gamma_c|), \quad \gamma < \gamma_c, \end{aligned} \quad (21)$$

with $\Im(\cdot)$ denoting the imaginary component.

We thus conclude that the bifurcation is characterized by a square-root singularity for both the coalescence of the real eigenvalues and for the bifurcation of the imaginary parts. We verify this prediction in Sec. VB.

IV. NUMERICAL MODEL

To demonstrate the predictions presented above (which are based on a linearized stability matrix) we employ the following numerical simulations. In addition, we will use numerical simulations to investigate the evolution of the instability away from the linear regime, where no theoretical predictions are available, as well as the effect of damping.

We focus on a specific example of a binary assembly of N frictional disks, half of which with radius $\sigma_1 = 0.5$ and the other half with $\sigma_2 = 0.7$, unit mass $m = 1$, and moment of inertia $I_i = 0.5m_i\sigma_i^2$. The normal interaction between the grains is given by Eq. (4), while the tangential interaction is given by Eq. (8), with $k_t = 2k_n/7$. We use m , $2\sigma_1$, and $\sqrt{m(2\sigma_1)^{-1/2}k_n^{-1}}$ as our units of mass, length, and time, respectively. We consider different values for the friction coefficient μ and the system size N .

The equations of motion are solved using two types of algorithms: ‘‘Newtonian’’ and ‘‘overdamped.’’ The first is simply a solution of the Newton equations of motion with the given forces Eqs. (4) and (8). The second algorithm solves the same equations of motion but with a damping force that is proportional to the velocities of the disks with a coefficient of proportionality $\eta_v = m\eta_0$. If not otherwise mentioned, we use $\eta_0 = 2.2 \times 10^{-2}$ expressed in reduced units. This value of η_0 ensures that the dynamics is overdamped, as the damping timescale η_v^{-1} is of the order of the time that sounds needs to travel one particle diameter. In the overdamped limit, even in the presence of complex eigenvalues the oscillatory instability is suppressed, as accelerations can be neglected and the equations of motion become of first order. We use LAMMPS [35] to perform the numerical integration for these two algorithms, with an integration time step of $10^{-5} \sqrt{(2\sigma_1)^{1/2}k_n m^{-1}}$.

V. CRITICAL FEATURE OF THE INSTABILITY

A. Birth of complex conjugate pairs

To demonstrate the instability mechanism and describe its critical features, we start recapping the results of Ref. [32] with regard to the emergence of a pair of complex eigenvalues. An initial configuration is prepared by arranging binary particles randomly in a two-dimensional box and then perform two consecutive runs of overdamped dynamics to bring the configuration at mechanical equilibrium. The initial configuration is prepared by focusing on a frictionless system (i.e., $\mu = 0$) and hence has no complex eigenvalues. Afterwards, we switch on friction and perform athermal quasi static (AQS) simulations: starting from the initial stable configuration, we shear the simulation box along the horizontal direction (x) by the amount $\delta\gamma$ and then we run the overdamped dynamics until the system reaches mechanical equilibrium. Operatively, we consider the system to be in mechanical equilibrium when the net force on each particle is less than 5×10^{-14} . Here $\delta\gamma$ varies in the range 10^{-4} – 10^{-6} , depending on the precision needed for the identification of the instability. After every AQS step we diagonalize the matrix \mathbf{J} to find its eigenvalues. At some value of γ we find the birth of a conjugate pair of complex eigenvalues, as seen in Fig. 1. If we continue to increase the strain using the same protocol, we see the continuous emergence of other complex pairs as well as the death of existing ones. We note that we observe complex eigenvalues, which corresponds to an unstable system, as we are using in this investigation an overdamped dynamics which kills the growth of the instability. The effect of damping is discussed in Sec. VII

B. Numerical tests of the universal square-root singularity

The calculation in Sec. III C shows that the approach to the instability has critical features. Here we examine the numerical ramifications of this criticality. We note that when the strain is increased, two real eigenvalues can collide to produce a complex conjugate pair, but the opposite can also happen as long as we increase the strain subject to overdamping; a pair of complex conjugate pairs can give rise to two real eigenvalues. The square-root singularity applies to both transitions.

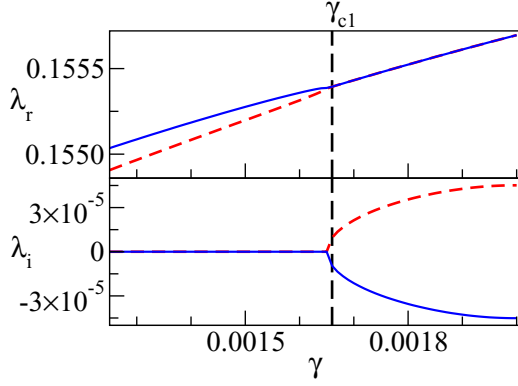


FIG. 1. Upon increasing the strain γ two modes with real eigenvalues λ coalesce at γ_{c1} (dashed vertical lines) and a pair of complex conjugate modes gets born. The upper and the lower panels show the evolution of the real and imaginary components of these modes for a system with $N = 500$, $\mu = 0.5$.

A good indicator for the birth and presence of two complex conjugate eigenfunctions over some range of strain values is provided by the scalar product of the two colliding modes. The scalar product of two eigenvectors is defined as $\langle u^m | u^n \rangle = |\sum_{j=1}^{3N} (u_{r,j}^m + i u_{i,j}^m)(u_{r,j}^n + i u_{i,j}^n)|$. $\langle u^m | u^n \rangle$ varies in the interval $[0, 1]$. At the critical value γ_c the scalar product reaches unity. This is quite obvious, since at the critical point the eigenfunctions also become complex conjugates. We show this first in Fig. 2 for a system of 10 disks and in Fig. 3 for 500 disks. Note that the eigenvectors of a real nonsymmetric matrix are linearly independent but in general not orthogonal.

A direct test of the universality predicted in the last section is provided by the difference between the two real eigenvalues. The data are consistent with $|\lambda_r^1 - \lambda_r^2| \propto (\gamma_c - \gamma)^x$, and $x \simeq 0.5$. This is shown in Fig. 4.

VI. DEVELOPMENT OF THE INSTABILITY

A. Linear response regime

To investigate the development of an instability, we consider the Newtonian (no damping) evolution of a configuration having a pair of complex conjugate eigenvalues. As long as the deviations from mechanical equilibrium are sufficiently

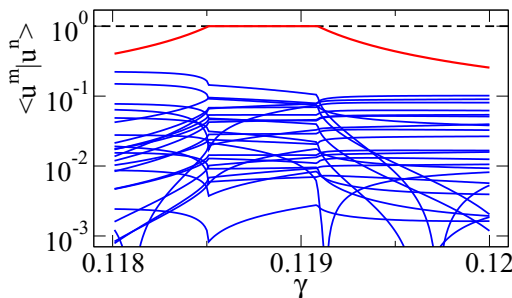


FIG. 2. Scalar products between the eigenvector $|u^m\rangle$ of a fixed mode m (here $m = 25$) and all the other eigenvectors (total 29) over shear strain γ for a system of 10 disks. The dashed line is added to guide the eye.

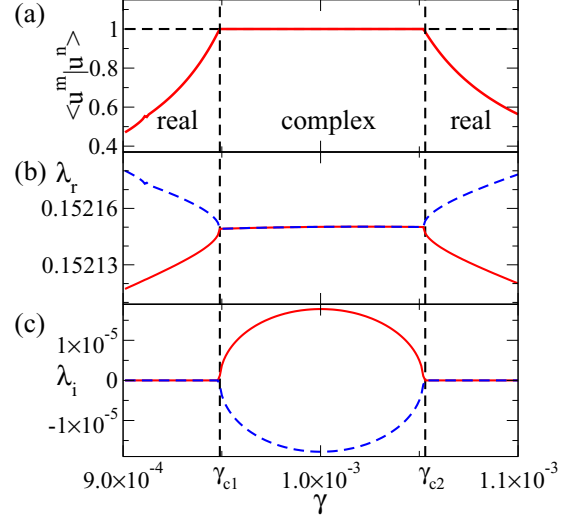


FIG. 3. (a) The scalar product of two eigenvectors for a system of $N = 500$ and $\mu = 10$. The two modes are complex conjugate in the strain interval varying between γ_{c1} and γ_{c2} . (b) The real and (c) the imaginary term of the two corresponding eigenvalues consistently show that these are complex conjugates for strain values in between γ_{c1} and γ_{c2} .

small, the eigenvalues and the eigenfunctions of \mathbf{J} furnish an accurate prediction for the developing instability. To see this we denote the complex mode m of \mathbf{J} whose complex eigenvalue $\lambda^m = \lambda_r + i\lambda_i$ is

$$|u^m\rangle = |u_r^m\rangle + i|u_i^m\rangle. \quad (22)$$

Since the dimension of \mathbf{J} is $3N \times 3N$, then $|u_r^m\rangle$ and similarly $|u_i^m\rangle$ have $3N$ components. As

$$\mathbf{J}|u^m\rangle = \lambda^m|u^m\rangle, \quad (23)$$

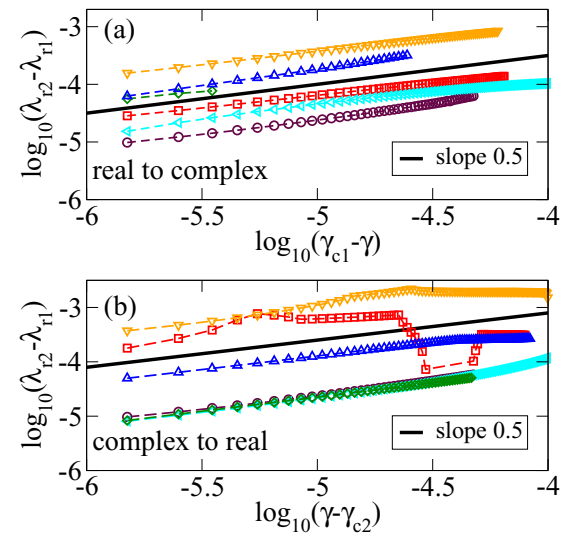


FIG. 4. Critical behavior of the difference between two real eigenvalues as they collide as γ approaches γ_{c1} (a) or depart as γ overcomes γ_{c2} . The different curves refer to events occurring in different samples with N (500, 1000) and μ (0.5, 10). The solid lines are straight lines with slope 0.5.

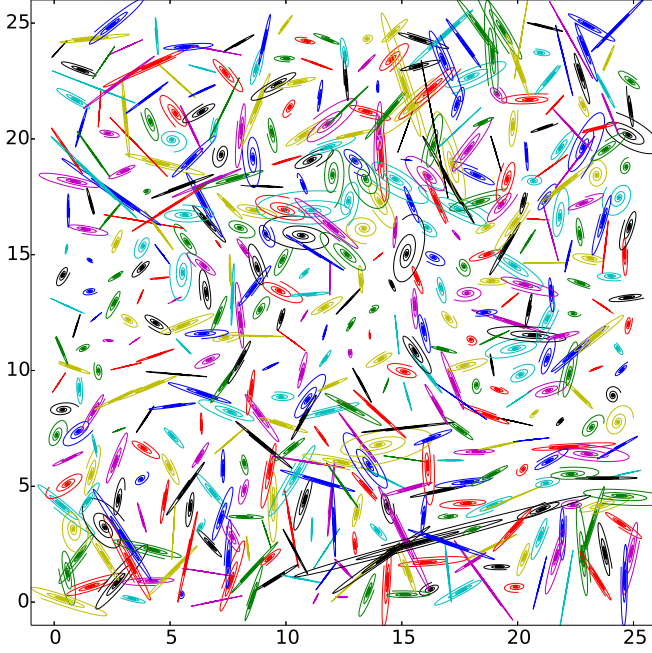


FIG. 5. A typical image of spiral trajectories of 500 disks in linear response regime. Here actual particle displacements are amplified by a factor of 10^6 .

we can rewrite the above equation in the form

$$\mathbf{J}|u_r^m\rangle = \lambda_r|u_r^m\rangle - \lambda_i|u_i^m\rangle, \quad (24)$$

$$\mathbf{J}|u_i^m\rangle = \lambda_i|u_r^m\rangle + \lambda_r|u_i^m\rangle. \quad (25)$$

In matrix notation this can be expressed as follows:

$$\mathbf{J}[\mathbf{u}_r^m \quad \mathbf{u}_i^m]_{3N \times 2} = [\mathbf{u}_r^m \quad \mathbf{u}_i^m]_{3N \times 2} \times \begin{bmatrix} \lambda_r & \lambda_i \\ -\lambda_i & \lambda_r \end{bmatrix}_{2 \times 2}. \quad (26)$$

The right-hand side of the above equation produces a dynamic matrix of dimension $3N \times 2$:

$$[\ddot{\mathbf{u}}^1 \quad \ddot{\mathbf{u}}^2]_{3N \times 2} = [\mathbf{u}_r^m \quad \mathbf{u}_i^m]_{3N \times 2} \times \begin{bmatrix} \lambda_r & \lambda_i \\ -\lambda_i & \lambda_r \end{bmatrix}_{2 \times 2}. \quad (27)$$

In particular, under the operation of this matrix, the resultant of $\ddot{\mathbf{u}}^1$ and $\ddot{\mathbf{u}}^2$, i.e.,

$$\ddot{\mathbf{u}}^m = \ddot{\mathbf{u}}^1 + \ddot{\mathbf{u}}^2, \quad (28)$$

is subject to a rotation-scaling operation and is therefore expected to predict a spiral trajectory with exponentially increasing speed. To demonstrate this, we consider a system in equilibrium and set the velocities of the particles (both translational and rotational) along the direction fixed by $\ddot{\mathbf{u}}^m$ and then follow the evolution of the system. Figure 5 clearly shows that particles display the expected spiral motion. The corresponding evolution of the mean square displacement of the center of mass $M(t)$ and the mean square change in the angular coordinate $A(t)$ can also be determined. Denoting

$$\begin{aligned} \Delta r_i^x(t) &\equiv r_i^x(t) - r_i^x(t=0), \\ \Delta r_i^y(t) &\equiv r_i^y(t) - r_i^y(t=0), \\ \Delta \theta_i(t) &\equiv \theta_i(t) - \theta_i(t=0), \end{aligned} \quad (29)$$

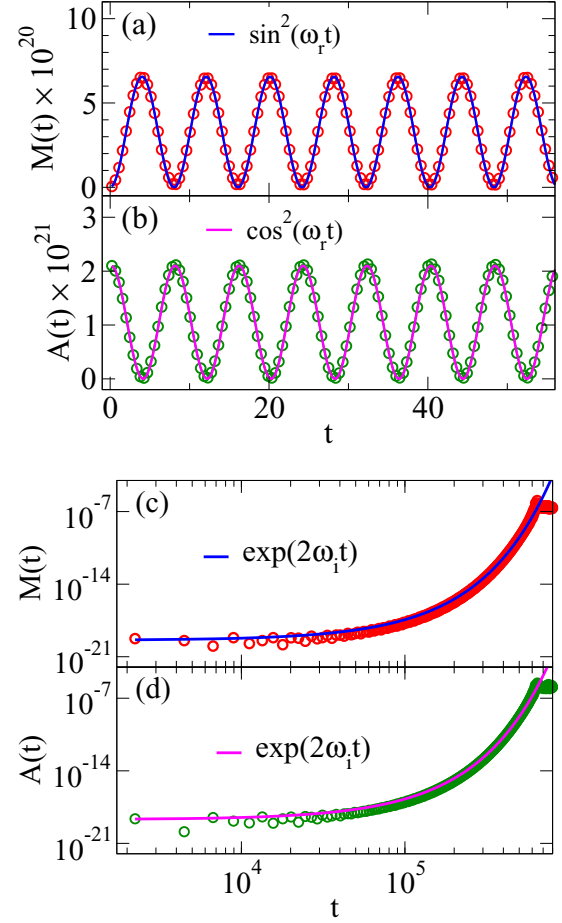


FIG. 6. (a) $M(t)$ and (b) $A(t)$ during the early stage of Newtonian dynamics after setting the velocities (both translation and rotation) of 500 disks along the resultant vector $\ddot{\mathbf{u}}^m$, Eq. (28). Both quantities display sinusoidal motion with the expected real eigenfrequency ω_r . (c) $M(t)$ and (d) $A(t)$ grow exponentially following the form $\sim \sin^2(\omega_r t + \phi) \exp(2\omega_r t)$, where ϕ is the initial phase, zero for $M(t)$ and $\pi/2$ for $A(t)$. The growth stops typically at $M(t) \sim 10^{-7}$ when either a few contacts break or a few new contacts are created.

we define

$$\begin{aligned} M(t) &\equiv \frac{1}{N} \sum_i^N [(\Delta r_i^x(t))^2 + (\Delta r_i^y(t))^2], \\ A(t) &\equiv \frac{1}{N} \sum_i^N (\Delta \theta_i(t))^2. \end{aligned} \quad (30)$$

According to Eq. (13), the system should behave as $M(t) \propto A(t) \propto e^{2\omega_r t} \sin^2(\omega_r t)$. As shown in Fig. 6, both quantities display sinusoidal motion since the beginning of the Newtonian dynamics with the expected frequency ω_r and the expected exponential growth $e^{2\omega_r t}$.

B. The nonlinear regime

When the instability develops sufficiently, the system exits from the linear response regime. It is of interest to consider how this happens and what is the long-time fate of the instability. We address this point following the evolution

of a number of unstable configurations in which the linear instability is associated with complex eigenvalues with very different frequencies. It is noteworthy that while these initial configurations usually have more than a single pair of complex eigenfunctions, the dynamics in the linear regime is dominated by the complex mode with the largest ω_i , which defines the growth rate of the instability. We illustrate the evolution of these different systems in Fig. 7, which reports the time evolution of the mean square displacement (a), of the pressure (b), and of the shear stress (c). From these figures, we identify in the dynamics the following regimes:

(1) A transient regime where the mean square displacement $M(t)$ grows subdiffusively, approximately as a power law. This growth, which is minute in magnitude, $M(t) < 10^{-22}$, might originate from the excitation of stable modes due to numerical noise.

(2) The effect of the oscillatory instabilities becomes dominant when time reaches $\sim \omega_i^{-1}$. An exponential growth is evident as expected in $M(t) \sim \sin^2(\omega_i t) \exp(2\omega_i t)$. Similarly, as illustrated in the inset of Fig. 7(b), the pressure P oscillates around its initial value with the oscillation amplitude increasing exponentially as $P(t) - P(0) \sim \sin(\omega_i t) \exp(\omega_i t)$. The dashed lines in the inset illustrate the envelope $\pm \exp(\omega_i t)$, where $\omega_i \sim 2.3 \times 10^{-5}$. The shear stress is also oscillating as the pressure around a constant value in the linear response regime, already shown explicitly in [32].

(3) The exponential growth is interrupted when $M(t) \sim 10^{-7}$, which occurs at a characteristic time proportional to ω_i^{-1} . At this time the two unstable complex conjugate modes annihilate as a consequence of the breaking of a few contacts (see below) and $M(t)$ enters a plateau regime. In this plateau regime, P and σ exhibit enhanced fluctuations but no noticeable change in their mean values.

(4) The plateau regime is interrupted by a fast growth of $M(t)$ driven by a second instability, which is triggered by the emergence of a number of complex eigenvalues. Afterward, the system enters a diffusive regime. This second instability leads to a sharp increase in the pressure and to a dramatic drop in shear stress σ_{xy} .

Figure 8 illustrates how the development of the instability is related to the change in the spectrum. The inset follows the evolution of the imaginary part of the complex eigenvalues dominating at short time and shows that this vanishes when the exponential growth phase ends for the considered $\omega_i \sim 2.3 \times 10^{-5}$. The main panel follows the evolution of the imaginary part of all eigenvalues and demonstrates that the secondary instability is triggered by the emergence of several unstable modes. The two consecutive vertical black dashed lines in Fig. 8 represent the end of the exponential growth and the beginning of the second instability.

The comparison of Fig. 8 and Figs. 7(b) and 7(c) clarifies that the effect of a dying complex mode might be eventful from a mechanical viewpoint. On the one hand, it activates many new complex modes. On the other hand, the shear stress σ_{xy} drops almost to zero. Regarding the structure of the system, we observe in Fig. 9(a) that the end of the exponential growth is associated with the destruction of a few contacts. In addition, a few contacts achieve the Coulomb threshold (inset). A significant restructuring of the contact network occurs only during the second instability, which is associated with a

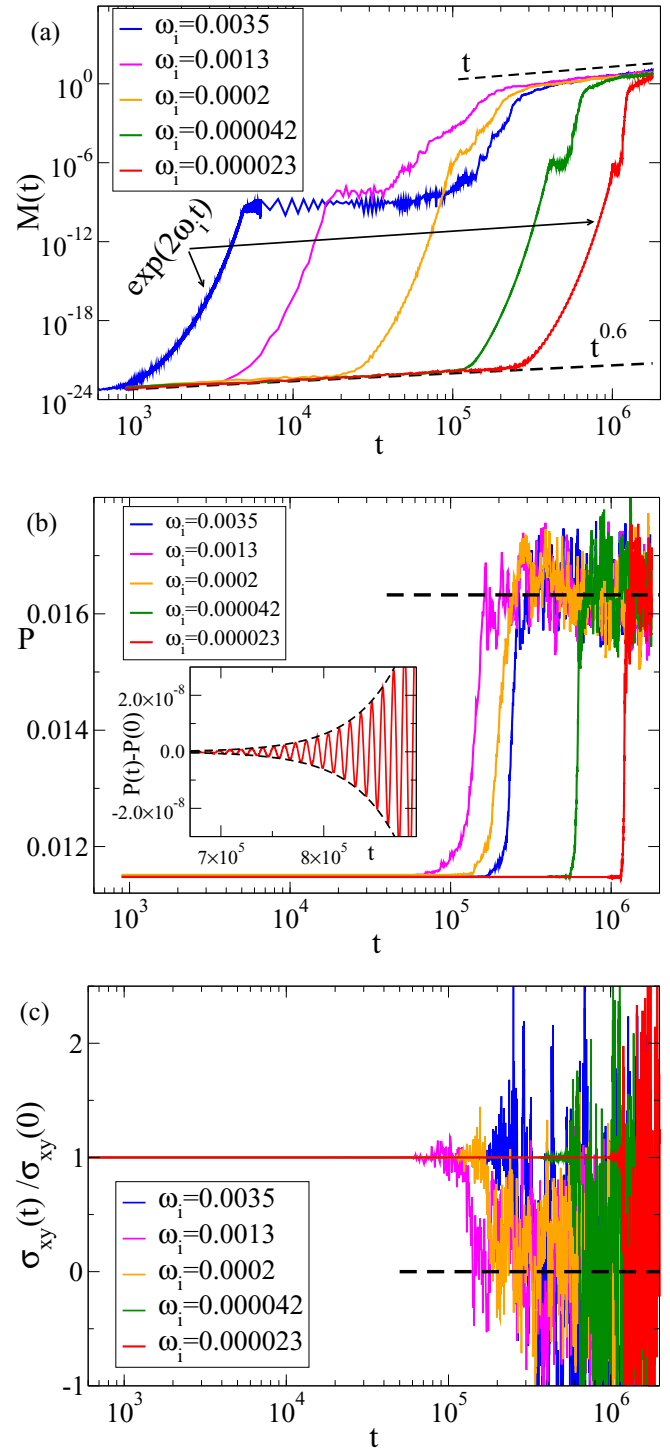


FIG. 7. Long-time fate of the oscillatory instability evolving with a Newtonian dynamics for $N = 500$ and $\mu = 10$. Different lines correspond to different initial configurations, identified by their complex eigenvalue with the largest imaginary component (growth rate). (a) Mean square displacement $M(t)$, (b) pressure P , and (c) shear stress σ_{xy} . Inset of (b) P (solid line) in the linear response regime for $\omega_i \sim 2.3 \times 10^{-5}$. Two dashed lines are $\pm \exp(\omega_i t)$ functions.

drop in the number of contacts between grains. This drop leads to a significant change in the probability distribution of the number of contacts per particle, $P(z_i)$, due to the emergence of particles with few contacts, as in Fig. 9(b).

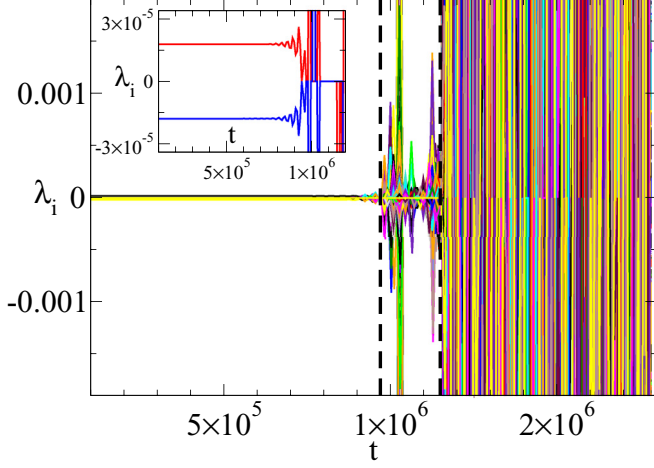


FIG. 8. Evolution of the $3N = 1500$ imaginary component of the eigenvalues λ_i during a Newtonian dynamics. The initial configuration contains one single pair of complex eigenpairs with $\omega_i \sim 2.3 \times 10^{-5}$, whose evolution is illustrated in the inset. The left vertical dashed line signifies the end of the existing complex eigenpair that further coincides with the end of exponential growth in $M(t)$. The right vertical dashed line signifies the birth of many complex eigenpairs that initiates the second instability in $M(t)$, see Fig. 7.

We finally clarify that the sharp increase in the pressure observed during the second instability is associated with the fluidization of the system. To this end, we introduce a per-particle pressure defined as $P_i = \frac{1}{4L^2} \sum_{j=1}^N \mathbf{r}_{ij} \cdot \mathbf{F}_{ij}$ such that $P = \sum_{i=1}^N P_i$. Figure 10(a) illustrates the distribution of $P_{ij} = \mathbf{r}_{ij} \cdot \mathbf{F}_{ij}$ at time $t = 0$ and at a later time after the secondary instability. Clearly, in the final state the pressure distribution

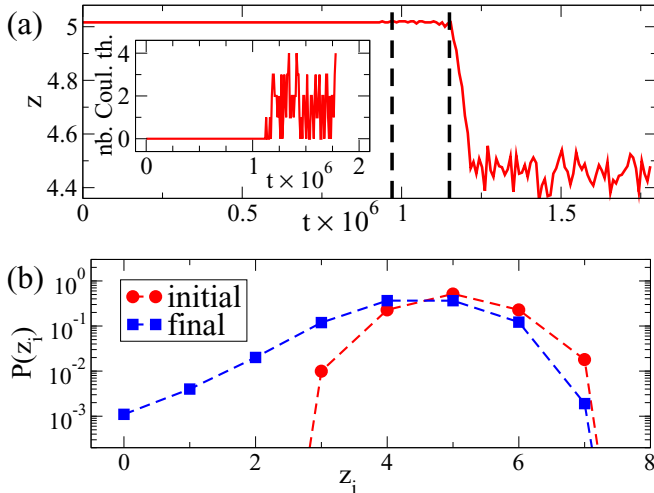


FIG. 9. Newtonian dynamics. (a) Number of contacts z on average a disk has exhibiting a sharp drop at second instability shown in Fig. 7. The dashed lines correspond to (i) the collapse of the initial complex pair that coincides with a few make or break contacts and (ii) birth of many complex modes coincides with the verge of the drop in contacts, see Fig. 8. (Inset) Number of contacts are at the Coulombic threshold. (b) The probability distribution function for a disk to have z contacts before and after the drop.

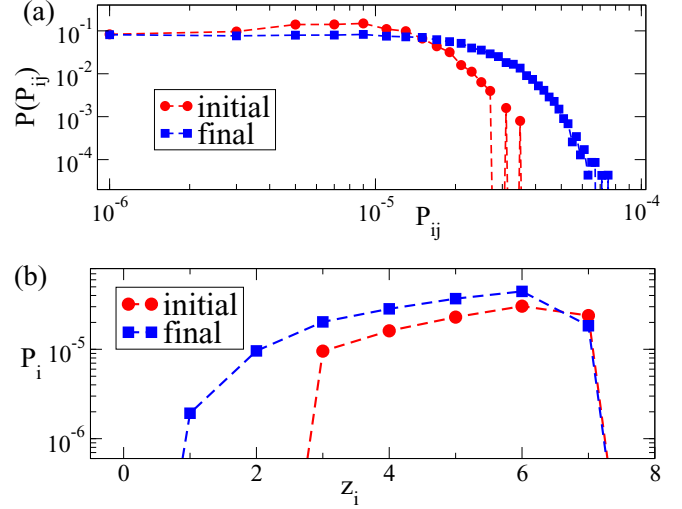


FIG. 10. Newtonian dynamics: (a) the distribution of binary pressure P_{ij} and (b) the pressure P_i exerted on each particle having contacts z before and after the nonlinear dynamics, see text for details.

has a longer tail, consistent with the observation of a larger average pressure value. Figure 10(b) illustrates the average value of P_i of the particles having z contacts. In the final configuration, the pressure is higher for all values of z as a consequence of the existence of large particle deformation associated with the flow of the system.

VII. THE EFFECTS OF DAMPING

While we have investigated the development of the oscillatory instability solving Newton's equations with no dissipation, in most real system applications there is some form of damping. It can be due to the water and grit in a fault, to the interparticle interaction, or to additional friction with a confining substrate. It is therefore important to ask if and how damping affects the observed instabilities.

We have clarified in Sec. IV that the instability disappears in the truly overdamped limit as the equations of motion become first order. Here we show that a finite damping tames but does not kill the instability. In particular, the instabilities associated with a small exponential growth rate (and hence emerging from the collision of low-frequency modes) are more affected by the damping.

For our investigation we consider a starting configuration obtained from our athermal quasistatic simulations, which has a complex eigenpair with eigenfrequency $\omega_r \pm i\omega_i = 0.390\,064\,3 \pm i0.000\,022\,8$. We then evolve the system according to a Newtonian dynamics, where in Eq. (9) we add a damping force $-\tilde{m}_i \eta_0 \dot{\mathbf{r}}_i$ on the right-hand side. Figure 11 shows that the evolution of this damped dynamics depends on how the damping rate η_0 compares with the instability growth rate ω_i , focussing on the time dependence of the mean square displacement (a) and of the pressure (P). For $\eta_0 \gtrsim \omega_i$, the exponential growth is suppressed. For $\eta_0 < \omega_i$, the dynamics has all the same features we have found in Fig. 7. As an example, in the inset of the lower panel we show that the pressure P oscillates around its initial value

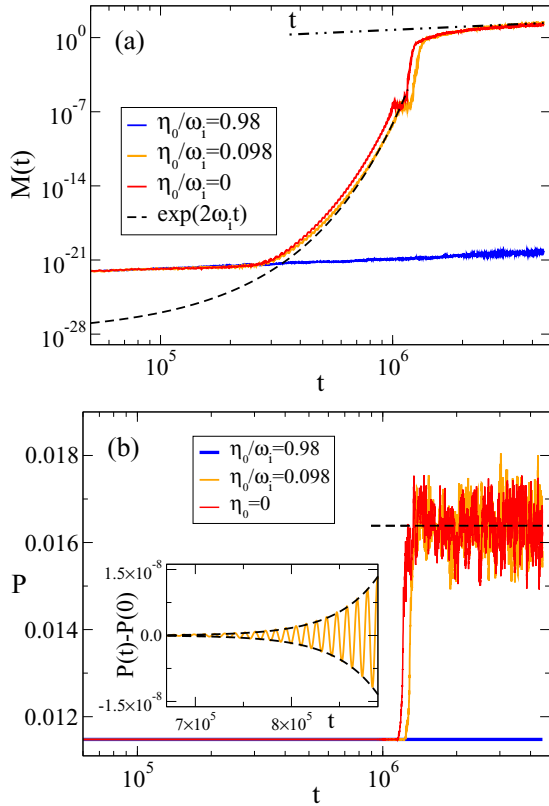


FIG. 11. The effect of damping on complex eigenfrequency. (a) Mean square displacement $M(t)$ and (b) pressure P display the same characteristic behaviors as for zero damping force when the damping frequency η_0 is smaller than the complex eigenfrequency ω_i .

while the oscillation amplitude increases exponentially as $P(t) - P(0) \sim \sin(\omega_i t) \exp(\omega_i t)$, as observed in the absence of damping in Fig. 7(b). Overall, this analysis clarifies that damping suppresses the instabilities with a small growth rate ω_i , not those corresponding to a large growth rate ω_i . Let us finally mention that we have explicitly checked that the instability occurs for damping values typical of granular systems [32].

VIII. HOW GENERIC IS THE OSCILLATORY INSTABILITY?

Having presented the oscillatory instability and its ability to self-amplify small perturbations, it is important to ask how generic is this instability. In particular, is the oscillatory instability a consequence of the structure of the Hertz-Mindlin model, as interpreted, for example, by Cundall and Strack [36], or is it expected to appear in any dynamical model of frictional disks. The answer to this question depends on what we mean by “a model” of frictional disks. During the last few decades the granular community has accepted that assemblies of disks can be described by coarse-grained coordinates, for example, the coordinates r_i of the centers of mass and θ_i for the angle of the disk [with reference to an initial angle $\theta_i(t = 0)$]. From the knowledge of these coordinates one writes down a physical model of the normal and

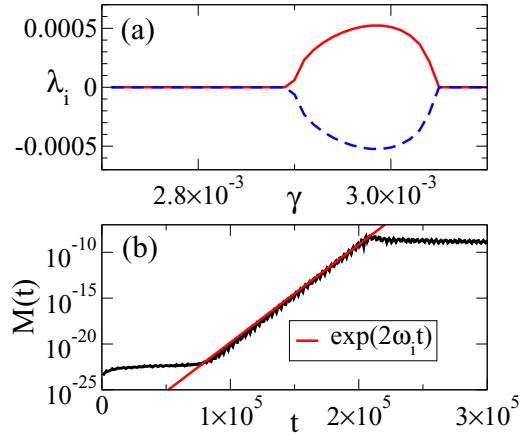


FIG. 12. (a) The typical characteristic of a complex eigenpair during an AQS simulation is recovered for a granular assembly of 500 particles where the normal interaction force is a harmonic function $k_n \delta$, and the tangential force is a smooth and continuous function $k_t [1 + (t/t^*) - (t/t^*)^2] t$, and at Coulomb threshold $t = t^*$, it is $\mu k_n \delta$ with $\mu = 10$. (b) Newtonian dynamics displays an exponential growth in mean square displacement, as expected for a system initially having a complex eigenpair.

tangential forces at each contact between neighboring disks. The other possibility is to track the exact microdynamics at each contact, paying attention to its leading and trailing edges, and taking into account the roughness of the contact and the plastic and elastic events that take place. This approach is not realistic for large assemblies of frictional disks and even less so for arbitrarily shaped granules. Thus, if one follows the approach of coarse-grained coordinates, the options are somewhat limited. Imagine, for example, that we decide to use the harmonic-type normal interaction and delete the $\sqrt{\delta_{ij}}$ term from the tangential force in Eq. (6). Then, on the face of it, the forces could be derived from a Hamiltonian of the form

$$U(\delta_{ij}, t_{ij}) = \frac{1}{2} k_n (\delta_{ij})^2 + \frac{1}{2} k_t (t_{ij})^2. \tag{31}$$

Will this suffice to eliminate the oscillatory instability? The answer is no, as long as we do not remove the Coulomb law and the requirement of smoothness of forces to allow derivatives. We stress here that any smoothing of the type done in Eq. (8) brings back the dependence of the tangential force on the normal force and makes the system non-Hamiltonian.

To demonstrate this, we have rerun our dynamics after removing the term $\sqrt{\delta_{ij}}$ from the tangential force in Eq. (6) but keeping the smoothing of this force at the Coulomb threshold. The resulting oscillatory instability is displayed in Fig. 12. As explained, the system still does not have a Hamiltonian structure, and the oscillatory instability remains generic. To drive home the message even further, we now remove the requirement of a smooth tangential force at the Coulomb threshold, allowing the tangential force to reach the limit in an abrupt way. Now the oscillatory instability disappears, since the Hamiltonian (31) now remains valid all the way to the Coulomb threshold. The price is, of course, that the Jacobian matrix J does not exist since the tangential force is not derivable at the threshold.

The above findings lead us to an interesting juncture for studying frictional properties in granular materials. The Hamiltonian models which oversimplify the role of deformation between two particles on static friction do not possess the oscillatory instabilities. In reality, the deformation between contacts is complex, as found by various experiments and atomistic simulations, and a direct intrusion of overlap distance in the tangential force is the culmination of this fact. The overall dynamics becomes a non-Hamiltonian that further displays oscillatory instabilities with a cost of no guarantee in energy conservation. At this point one depends on experiments to verify or refute the existence of this micromechanics in granular materials.

IX. SUMMARY AND THE ROAD AHEAD

It appears from our discussion that oscillatory instabilities should be expected as a generic feature present in physical systems whose dynamics are not derivable from a Hamiltonian. This instability was recently reported for frictional assemblies of disks [32]. In this article, we have explored further the characteristics and the consequences of such instabilities on similar frictional granular systems.

We have shown that the birth and death of an oscillatory instability upon athermal quasistatic shear are a critical phenomenon. A pair of complex eigenpairs is born when two real eigenmodes align to one another; the relative difference between the two real eigenvalues vanishes with shear strain following a power law function with exponent 1/2. Similarly, the death of the complex eigenpair takes place when the alignment between the two eigenvectors is lost. The relative difference between the two real eigenvalues gradually increases following the same power law as a function of the strain.

With Newtonian dynamics the presence of a complex eigenpair generates instabilities where the oscillatory amplitudes increase exponentially. During this linear response regime, particles move in spiral trajectories whose directions are determined by the two complex eigenvectors of the corresponding eigenpair. We have presented a formalism describing the direction of the spiral trajectories in the real plane; it is determined by the two complex eigenvectors. The linear response regime comes to an end when the oscillatory amplitude becomes so large that it breaks or makes a few pair contacts. This has a dramatic consequence, triggering a second instability due to which the system goes through a structural change. The number of contacts of a particle becomes broadly distributed, resulting in an increase of pressure. The dynamics becomes diffusive, helping the system to dissipate the shear stress. The above phenomena are generic for a whole range of complex eigenvalues and even in the presence of damping force, as long as the damping frequency is smaller than the imaginary eigenfrequency.

Probably the most important conclusion is that we have uncovered here a mechanism for a giant amplification of small perturbations. This finding may have further consequences in the context of a number of physics problems that involve frictional interactions. One fundamental question is how static friction turns into dynamical friction [37–39]. So far it is not quite clear what is the precise instability that allows two

compressed interfaces to start moving with respect to one another. It is worthwhile in the near future to examine whether the type of instability discussed above may be responsible for setting in this interesting transition. Another context of interest is that of remote triggering. It is known that one earthquake can induce another earthquake far away [28,40,41]. Since strong seismic waves are strongly damped, only weak perturbation can travel a long distance. So the phenomenon of remote triggering requires a mechanism for self-amplification. While we are fully aware that geological faults are very much more complex than assemblies of frictional disks, it appears highly worthwhile to explore the relevance of the kind of self-amplification of small perturbation discussed above as it relates to the problem of remote triggering. It is certainly on our agenda in the near future.

ACKNOWLEDGMENTS

This work had been supported in part by the ISF-Singapore exchange program and by the US-Israel Binational Science Foundation. We thank Jacques Zylberg and Yoav Pollack for useful discussions and exchanges at the early stages of this project. J.C. and M.P.C. acknowledge NSCC Singapore for granting the computational facility.

APPENDIX: CALCULATION OF THE OPERATOR J

The Jacobian operator J , which is the dynamical response of the system, represents the derivative of the forces and of the torques acting on the particles with respect to all the degrees of freedom. The interaction forces used in this study are recalled in subsection 1 of Appendix then the expression of the tangential displacement and its derivative in (subsection 2 of Appendix), and the derivatives of forces and torques with respect to generalized coordinates in (subsection 3 of Appendix) are stated. Finally, we show the expressions for all the components of J subsection 4 of Appendix and how these components are arranged as a matrix (subsection 5 of Appendix).

1. Interaction force

In our simulation, a pair of granular particles interacts when they overlap. The overlap distance δ_{ij} is measured as

$$\delta_{ij} = \sigma_i + \sigma_j - r_{ij}, \quad (\text{A1})$$

where r_{ij} is the center-to-center distance of a pair i and j , and σ_i is the radius of particle i . The pair vector \mathbf{r}_{ij} is defined as

$$\mathbf{r}_{ij} = \mathbf{r}_i - \mathbf{r}_j. \quad (\text{A2})$$

The pair-interaction force \mathbf{F}_{ij} has two contributions: $\mathbf{F}_{ij}^{(n)}$ is the force acting along the normal direction of the pair $\hat{\mathbf{r}}_{ij}$, and $\mathbf{F}_{ij}^{(t)}$ is the force acting along the tangential direction of the pair $\hat{\mathbf{t}}_{ij}$. The normal force is Hertzian,

$$\mathbf{F}_{ij}^{(n)} = k_n \delta_{ij}^{3/2} \hat{\mathbf{r}}_{ij}, \quad (\text{A3})$$

where k_n is the force constant with dimension: force per length^{3/2}. The tangential force $\mathbf{F}_{ij}^{(t)}$ is a function of both the overlap distance δ_{ij} and the tangential displacement \mathbf{t}_{ij} . We have modified the standard expression for $\mathbf{F}_{ij}^{(t)}$ and included a few higher-order terms of \mathbf{t}_{ij} (i.e., $|\mathbf{t}_{ij}|$) such that the derivative

of the force function $F_{ij}^{(t)}$ with respect to tangential distance t_{ij} becomes continuous and it goes to zero smoothly. We use the following form:

$$\begin{aligned} \mathbf{F}_{ij}^{(t)} &= -k_t \delta_{ij}^{1/2} \left[1 + \frac{t_{ij}}{t_{ij}^*} - \left(\frac{t_{ij}}{t_{ij}^*} \right)^2 \right] t_{ij} \hat{\mathbf{r}}_{ij} \\ &= -k_t \delta_{ij}^{1/2} t_{ij}^* \hat{\mathbf{r}}_{ij}, \quad \text{if } k_t \delta_{ij}^{1/2} t_{ij} > \mu |\mathbf{F}_{ij}^{(n)}|, \end{aligned} \quad (\text{A4})$$

where k_t is the tangential force constant. Its dimension is force per length^{3/2}. t_{ij}^* is the threshold tangential distance:

$$t_{ij}^* = \mu \frac{k_n}{k_t} \delta_{ij}, \quad (\text{A5})$$

where μ is the friction coefficient, a scalar quantity which essentially determines the maximum strength of the tangential force with respect to the normal force at a fixed overlap δ_{ij} . The derivative of $F_{ij}^{(t)}$ with respect to t_{ij} vanishes at t_{ij}^* , as it turns out

$$\begin{aligned} \frac{\partial F_{ij}^{(t)}}{\partial t_{ij}} &= k_t \delta_{ij}^{1/2} \left[1 + 2 \frac{t_{ij}}{t_{ij}^*} - 3 \left(\frac{t_{ij}}{t_{ij}^*} \right)^2 \right] \\ &= 0, \quad \text{if } k_t \delta_{ij}^{1/2} t_{ij} > \mu |\mathbf{F}_{ij}^{(n)}|. \end{aligned} \quad (\text{A6})$$

We stress here that the above forces imply a non-Hamiltonian dynamics. That is, there is not a function $U(\delta, t)$ such that $F^{(n)} = -\frac{\partial U}{\partial \delta}$ and $F^{(t)} = -\frac{\partial U}{\partial t}$.

2. Tangential displacement

The tangential force is a function of both t_{ij} and \mathbf{r}_{ij} . The derivative of this force thus includes the derivative of the two latter quantities. Here we evaluate these derivatives using the chain rule.

The derivative of tangential displacement t_{ij} with respect to time t is

$$\frac{dt_{ij}}{dt} = \mathbf{v}_{ij} - \mathbf{v}_{ij}^n + \hat{\mathbf{r}}_{ij} \times (\sigma_i \boldsymbol{\omega}_i + \sigma_j \boldsymbol{\omega}_j), \quad (\text{A7})$$

where $\mathbf{v}_{ij} = \mathbf{v}_i - \mathbf{v}_j$ is the relative velocity of pair i and j . \mathbf{v}_{ij}^n is the projection of \mathbf{v}_{ij} along the normal direction $\hat{\mathbf{r}}_{ij}$. $\mathbf{v}_{ij} - \mathbf{v}_{ij}^n$ is the tangential component of the relative velocity. $\boldsymbol{\omega}_i$ and $\boldsymbol{\omega}_j$ are the angular velocity of i and j , respectively. In differential form, the above equation reads

$$dt_{ij} = d\mathbf{r}_{ij} - (d\mathbf{r}_{ij} \cdot \hat{\mathbf{r}}_{ij}) \hat{\mathbf{r}}_{ij} + \hat{\mathbf{r}}_{ij} \times (\sigma_i d\boldsymbol{\theta}_i + \sigma_j d\boldsymbol{\theta}_j), \quad (\text{A8})$$

where $d\boldsymbol{\theta}_i$ is the angular displacement of i , which follows the relation $d\boldsymbol{\omega}_i = \frac{d\boldsymbol{\theta}_i}{dt}$.

From here forward, we assume the two-dimensional (2D) system. Therefore, $\boldsymbol{\omega}_i$, and so $\boldsymbol{\theta}_i$, have only one compo-

nent along $\hat{\mathbf{z}}$, perpendicular to the xy plane, and $\hat{\mathbf{r}}_{ij} \times d\boldsymbol{\theta}_i = d\theta_i (\mathbf{y}_{ij} \hat{\mathbf{x}} - \mathbf{x}_{ij} \hat{\mathbf{y}}) / r_{ij}$. This allows one to write Eq. (A8) as

$$dt_{ij}^\alpha = dr_{ij}^\alpha - (d\mathbf{r}_{ij} \cdot \hat{\mathbf{r}}_{ij}) \frac{r_{ij}^\alpha}{r_{ij}} + (-1)^\alpha (\sigma_i d\theta_i + \sigma_j d\theta_j) \frac{r_{ij}^\beta}{r_{ij}}, \quad (\text{A9})$$

where α and β can take values of 0 and 1, which correspond to the x and y components, respectively. Now if particle i changes its position, the angular displacement remains unaffected, i.e., $\frac{d\theta_i}{dr_i^\alpha} = 0$. Thus, the change in tangential displacement along β due to the change in position of particle i along α contributes only in translations, and it can be written as [using (A9)]

$$\frac{dt_{ij}^\beta}{dr_i^\alpha} = \Delta_{\alpha\beta} - \frac{r_{ij}^\alpha r_{ij}^\beta}{r_{ij}^2}, \quad (\text{A10})$$

where $\Delta_{\alpha\beta}$ is the Kronecker δ , which is 1 when $\alpha = \beta$, or else zero. Similarly, a change in rotational coordinates does not modify the particles' relative distance, i.e., $\frac{dt_{ij}^\beta}{d\theta_i} = 0$. Thus, the change in tangential displacement along β due to the change in θ_i is [from (A9)]

$$\frac{dt_{ij}^\beta}{d\theta_i} = (-1)^\beta \sigma_i \frac{r_{ij}^\alpha}{r_{ij}}. \quad (\text{A11})$$

In the above equation α and β are always different. Now the magnitude of tangential distance t_{ij} can be obtained from the relation $t_{ij}^2 = \sum_\alpha t_{ij}^{\alpha 2}$. Its differential follows $dt_{ij} = \sum_\alpha \frac{t_{ij}^\alpha}{t_{ij}} dt_{ij}^\alpha$. The derivatives of tangential distance t_{ij} with respect to r_i^α and θ_i can be expressed as

$$\frac{dt_{ij}}{dr_i^\alpha} = \left(\frac{t_{ij}^x}{t_{ij}} \right) \frac{dt_{ij}^x}{dr_i^\alpha} + \left(\frac{t_{ij}^y}{t_{ij}} \right) \frac{dt_{ij}^y}{dr_i^\alpha}, \quad (\text{A12})$$

$$\frac{dt_{ij}}{d\theta_i} = \left(\frac{t_{ij}^x}{t_{ij}} \right) \frac{dt_{ij}^x}{d\theta_i} + \left(\frac{t_{ij}^y}{t_{ij}} \right) \frac{dt_{ij}^y}{d\theta_i}. \quad (\text{A13})$$

With the help of Eqs. (A10) and (A11) we can solve the above two differential equations. As the tangential threshold is a linear function of overlap distance δ_{ij} [see (A5)], it also is modified due to a change in r_i^α as

$$\frac{dt_{ij}^*}{dr_i^\alpha} = -\mu \left(\frac{k_n}{k_t} \right) \frac{r_{ij}^\alpha}{r_{ij}}, \quad (\text{A14})$$

and it is unaffected by the change in rotation, i.e., $\frac{dt_{ij}^*}{d\theta_i} = 0$.

3. Evaluation of J

The derivative of tangential force [Eq. (A4)] with respect to r_i^α :

$$\begin{aligned} \frac{\partial F_{ij}^{(t)\beta}}{\partial r_i^\alpha} &= -k_t \frac{\partial}{\partial r_i^\alpha} \left[\delta_{ij}^{1/2} (t_{ij}^\beta + \tilde{t} t_{ij}^\beta - \tilde{t}^2 t_{ij}^\beta) \right] \\ &= -\frac{1}{2} \delta_{ij}^{-1} \frac{r_{ij}^\alpha}{r_{ij}} F_{ij}^{(t)\beta} - k_t \delta_{ij}^{1/2} \left[(1 + \tilde{t} - \tilde{t}^2) \frac{\partial t_{ij}^\beta}{\partial r_i^\alpha} + (\tilde{t}^\beta - 2\tilde{t}\tilde{t}^\beta) \frac{\partial t_{ij}}{\partial r_i^\alpha} + (-\tilde{t}\tilde{t}^\beta + 2\tilde{t}^2\tilde{t}^\beta) \frac{\partial t_{ij}^*}{\partial r_i^\alpha} \right]. \end{aligned} \quad (\text{A15})$$

Here we use the notation \tilde{t} to represent the ratio t_{ij}/t_{ij}^* and the notation \tilde{t}^β for t_{ij}^β/t_{ij}^* . The expressions for all three partial differentiations in (A15) are already shown in (A11), (A12), and (A14).

Similarly, the derivative of tangential force with respect to θ_i (using the same notation as above) can be found as

$$\frac{\partial F_{ij}^{(t)\beta}}{\partial \theta_i} = -k_t \delta_{ij}^{1/2} \left[(1 + \tilde{t} - \tilde{t}^2) \frac{\partial t_{ij}^\beta}{\partial \theta_i} + (\tilde{t}^\beta - 2\tilde{t}\tilde{t}^\beta) \frac{\partial t_{ij}}{\partial \theta_i} \right]. \quad (\text{A16})$$

From the above two equations it is then understood that if r_{ij} and t_{ij} are known the differential equations can be solved easily. When \tilde{t}^β is negligible for all β , then $\tilde{t} \approx 0$. This translates to $\frac{\partial F_{ij}^{(t)\beta}}{\partial \theta_i} = -(-1)^\beta k_t \sigma_i \delta_{ij}^{1/2} \frac{r_{ij}^\beta}{r_{ij}}$ with $\alpha \neq \beta$, implying that even in the case of zero tangential displacement and therefore, zero tangential force, the above derivative can be finite.

The derivative of normal force [Eq. (A3)] with respect to r_i^α is the following:

$$\frac{\partial F_{ij}^{(n)\beta}}{\partial r_i^\alpha} = k_n \frac{\partial}{\partial r_i^\alpha} \left[\delta_{ij}^{3/2} \frac{r_{ij}^\beta}{r_{ij}} \right] = k_n \delta_{ij}^{1/2} \left[\Delta_{\alpha\beta} \frac{\delta_{ij}}{r_{ij}} - \frac{3}{2} \frac{r_{ij}^\alpha r_{ij}^\beta}{r_{ij}^2} - \left(\frac{\delta_{ij}}{r_{ij}} \right) \frac{r_{ij}^\alpha r_{ij}^\beta}{r_{ij}^2} \right], \quad (\text{A17})$$

where $\Delta_{\alpha\beta}$ is the Kronecker δ . The derivative of total force, which reads

$$\frac{\partial F_{ij}^\beta}{\partial r_i^\alpha} = \frac{\partial F_{ij}^{(n)\beta}}{\partial r_i^\alpha} + \frac{\partial F_{ij}^{(t)\beta}}{\partial r_i^\alpha}, \quad (\text{A18})$$

$$\frac{\partial F_{ij}^\beta}{\partial \theta_i} = \frac{\partial F_{ij}^{(t)\beta}}{\partial \theta_i}, \quad (\text{A19})$$

can be solved using (A17), (A15), and (A16).

The torque of particle j due to tangential force $\mathbf{F}^{(t)}_{ij}$ is $\mathbf{T}_j = -\sigma_j (\hat{r}_{ij} \times \mathbf{F}^{(t)}_{ij}) \equiv \sigma_j \tilde{\mathbf{T}}_{ij}$. In 2D, $\tilde{\mathbf{T}}_{ij}$ has only a z component:

$$\tilde{T}_{ij}^z = - \left[\left(\frac{x_{ij}}{r_{ij}} \right) F_{ij}^{(t)y} - \left(\frac{y_{ij}}{r_{ij}} \right) F_{ij}^{(t)x} \right]. \quad (\text{A20})$$

The derivative of \tilde{T}_{ij}^z then becomes

$$\begin{aligned} \frac{\partial \tilde{T}_{ij}^z}{\partial r_i^\alpha} = & - \left(\frac{\delta_{\alpha x}}{r_{ij}} - \frac{x_{ij} r_{ij}^\alpha}{r_{ij}^3} \right) F_{ij}^{(t)y} - \left(\frac{x_{ij}}{r_{ij}} \right) \frac{\partial F_{ij}^{(t)y}}{\partial r_i^\alpha} \\ & + \left(\frac{\delta_{\alpha y}}{r_{ij}} - \frac{y_{ij} r_{ij}^\alpha}{r_{ij}^3} \right) F_{ij}^{(t)x} + \left(\frac{y_{ij}}{r_{ij}} \right) \frac{\partial F_{ij}^{(t)x}}{\partial r_i^\alpha}, \end{aligned} \quad (\text{A21})$$

where $\delta_{\alpha x}$ (similarly, $\delta_{\alpha y}$) is the Kronecker δ , such that $\delta_{xx} = 1$ and $\delta_{yx} = 0$, and

$$\frac{\partial \tilde{T}_{ij}^z}{\partial \theta_i} = - \left[\left(\frac{x_{ij}}{r_{ij}} \right) \frac{\partial F_{ij}^{(t)y}}{\partial \theta_i} - \left(\frac{y_{ij}}{r_{ij}} \right) \frac{\partial F_{ij}^{(t)x}}{\partial \theta_i} \right]. \quad (\text{A22})$$

The above two differential equations can be solved using Eqs. (A15) and (A16). If the tangential displacement t_{ij}^β is negligible compared to the threshold t_{ij}^* , $\tilde{t}^\beta \approx 0$ for all β . This results in $\tilde{t} \approx 0$. Therefore, $\frac{\partial \tilde{T}_{ij}^z}{\partial \theta_i} = k_t \sigma_i \delta_{ij}^{1/2}$.

4. Jacobian

The dimension of Jacobian operator J is force over length. To be consistent with the dimension we redefine the torque T

and rotational coordinate θ as

$$\tilde{T}_i = \frac{T_i}{\sigma_i}, \quad \text{and} \quad \tilde{\theta}_i = \sigma_i \theta_i. \quad (\text{A23})$$

In addition, the dynamic matrix has a contribution from the moment of inertia $I_i = I_0 m_i \sigma_i^2$ as $\Delta \omega_i = \mathbf{T}_i / I_i \Delta t$. In our calculation, we assume that mass m_i and I_0 both are 1. The remaining contribution of I_i , i.e., σ_i^2 , is taken care of by rescaling the torque and the angular displacement as \tilde{T}_i and $\tilde{\theta}_i$ (A23). For $I_0 \neq 1$, the contribution of I_0 can be correctly anticipated if we rewrite (A7) as below:

$$\frac{d\mathbf{t}_{ij}}{dt} = \mathbf{v}_{ij} - \mathbf{v}_{ij}^n + \frac{1}{I_0} \hat{r}_{ij} \times (\sigma_i \boldsymbol{\omega}_i + \sigma_j \boldsymbol{\omega}_j). \quad (\text{A24})$$

J essentially contains **four** different derivatives:

(1) First type—Derivative of force with respect to the position of particles:

$$\begin{aligned} J_{ij}^{\alpha\beta} &= \sum_{k=0; k \neq j}^{N-1} \frac{\partial F_{kj}^\beta}{\partial r_i^\alpha} = \frac{\partial F_{ij}^\beta}{\partial r_i^\alpha}, \quad \text{for } i \neq j \\ J_{ii}^{\alpha\beta} &= \sum_{j=0; j \neq i}^{N-1} \frac{\partial F_{ji}^\beta}{\partial r_i^\alpha} = - \sum_{j=0; j \neq i}^{N-1} J_{ij}^{\alpha\beta}, \end{aligned} \quad (\text{A25})$$

where N is the total number of particles. $J_{ij}^{\alpha\beta}$ is symmetric if we change pairs, i.e., $J_{ij}^{\alpha\beta} = J_{ji}^{\alpha\beta}$; however, the symmetry is not guaranteed with the interchange of α and β .

(2) Second type—Derivative of force with respect to the rotational coordinate:

$$\begin{aligned} J_{ij}^\beta &= - \sum_{k=0; k \neq j}^{N-1} \frac{\partial F_{kj}^\beta}{\partial \tilde{\theta}_i} = - \frac{\partial F_{ij}^\beta}{\partial \tilde{\theta}_i}, \quad \text{for } i \neq j \\ J_{ii}^\beta &= - \sum_{j=0; j \neq i}^{N-1} \frac{\partial F_{ji}^\beta}{\partial \tilde{\theta}_i} = - \sum_{j=0; j \neq i}^{N-1} J_{ij}^\beta. \end{aligned} \quad (\text{A26})$$

The negative sign makes sure that in stable systems all the eigenvalues are positive. J_{ij}^β is asymmetric: $J_{ij}^\beta = -J_{ji}^\beta$.

(3) Third type—Derivative of torque with respect to position:

$$J_{ij}^\alpha = \sum_{k=0; k \neq j}^{N-1} \frac{\partial \tilde{T}_{kj}^z}{\partial r_i^\alpha} = \frac{\partial \tilde{T}_j}{\partial r_i^\alpha}, \quad \text{for } i \neq j$$

$$J_{ii}^\alpha = \sum_{j=0; j \neq i}^{N-1} \frac{\partial \tilde{T}_{ji}^z}{\partial r_i^\alpha} = \sum_{j=0; j \neq i}^{N-1} J_{ij}^\alpha. \quad (\text{A27})$$

J_{ij}^α is also asymmetric: $J_{ij}^\alpha = -J_{ji}^\alpha$.

(4) Fourth type—Derivative of torque with respect to rotational coordinate:

$$J_{ij} = - \sum_{k=0; k \neq j}^{N-1} \frac{\partial \tilde{T}_{kj}^z}{\partial \theta_i} = - \frac{\partial \tilde{T}_j}{\partial \theta_i}, \quad \text{for } i \neq j$$

$$J_{ii} = - \sum_{j=0; j \neq i}^{N-1} \frac{\partial \tilde{T}_{ji}^z}{\partial \theta_i} = \sum_{j=0; j \neq i}^{N-1} J_{ij}. \quad (\text{A28})$$

The negative sign makes sure that in stable systems all the eigenvalues are positive. J_{ij} is symmetric: $J_{ij} = J_{ji}$.

5. Arrangement of Jacobian matrix

In two dimensions $D = 2$, for N particles the total number of elements in J is $(D + 1)N \times (D + 1)N$. In the matrix, first $DN \times DN$ elements contain the first type of force derivative, i.e., $J_{ij}^{\alpha\beta}$. Here the row index ro and column index co of J runs in the range $0 \leq ro < DN$ and $0 \leq co < DN$. Rows from $DN \leq ro < (D + 1)N$ and columns $0 \leq co < DN$ of J contain J_{ij}^β , i.e., the second type of derivative. Rows from $0 \leq ro < DN$ and columns $DN \leq co < (D + 1)N$ of J contain the third type J_{ij}^α . Finally, rows from $DN \leq ro < (D + 1)N$ and columns $DN \leq co < (D + 1)N$ of J hold J_{ij} , i.e., the fourth type of derivative. For a fixed type of derivative, at a fixed row, the column index first runs over j starting from 0 to $N - 1$. Then β is incremented, if it exists for that particular derivative type. Similarly, at a fixed column, the row index first runs over $i \in [0, N)$ and then α is incremented.

- [1] D. L. Malandro and D. J. Lacks, *Phys. Rev. Lett.* **81**, 5576 (1998).
- [2] D. L. Malandro and D. J. Lacks, *J. Chem. Phys.* **110**, 4593 (1999).
- [3] C. Maloney and A. Lemaître, *Phys. Rev. Lett.* **93**, 195501 (2004).
- [4] M. Wyart, *Ann. Phys. Fr.* **30**, 1 (2005).
- [5] S. Karmakar, E. Lerner, and I. Procaccia, *Phys. Rev. E* **82**, 026105 (2010).
- [6] H. G. E. Hentschel, S. Karmakar, E. Lerner, and I. Procaccia, *Phys. Rev. E* **83**, 061101 (2011).
- [7] I. Procaccia, C. Rainone, C. A. B. Z. Shor, and M. Singh, *Phys. Rev. E* **93**, 063003 (2016).
- [8] V. Dailidonis, V. Ilyin, I. Procaccia, and C. A. B. Z. Shor, *Phys. Rev. E* **95**, 031001(R) (2017).
- [9] R. Dasgupta, H. G. E. Hentschel, and I. Procaccia, *Phys. Rev. Lett.* **109**, 255502 (2012).
- [10] R. Dasgupta, H. G. E. Hentschel, and I. Procaccia, *Phys. Rev. E* **87**, 022810 (2013).
- [11] R. Dasgupta, O. Gendelman, P. Mishra, I. Procaccia, and C. A. B. Z. Shor, *Phys. Rev. E* **88**, 032401 (2013).
- [12] R. Mindlin, *Trans. ASME* **16**, 259 (1949).
- [13] O. R. Walton and R. L. Braun, *J. Rheol.* **30**, 949 (1986).
- [14] J. Jacques Moreau, *Eur. J. Mech. A. Solids* **13**, 93 (1994).
- [15] L. Vu-Quoc and X. Zhang, *Mech. Mater.* **31**, 235 (1999).
- [16] L. Vu-Quoc, X. Zhang, and L. Lesburg, *J. Appl. Mech.* **67**, 363 (2000).
- [17] L. E. Silbert, D. Ertaş, G. S. Grest, T. C. Halsey, D. Levine, and S. J. Plimpton, *Phys. Rev. E* **64**, 051302 (2001).
- [18] R. M. Nedderman, *Statics and Kinematics of Granular Materials* (Cambridge University Press, Cambridge, 1992).
- [19] S. McNamara, R. García-Rojo, and H. Herrmann, *Phys. Rev. E* **72**, 021304 (2005).
- [20] P. R. Welker and S. C. McNamara, *Phys. Rev. E* **79**, 061305 (2009).
- [21] P. Cundall and O. Strack, in *Mechanics of Granular Materials*, Studies in Applied Mechanics Vol. 7, edited by J. T. Jenkins and M. Satake (Elsevier, New York, 1983), pp. 137–149.
- [22] L. Staron, F. Radjai, and J.-P. Vilotte, *Eur. Phys. J. E* **18**, 311 (2005).
- [23] L. Staron, F. Radjai, and J.-P. Vilotte, *J. Stat. Mech.: Theory Exp.* (2006) P07014.
- [24] R. Hill, *J. Mech. Phys. Solids* **6**, 236 (1958).
- [25] F. Nicot, N. Hadda, L. Sibille, F. Radjai, and F. Darve, *C. R. Mécanique* **342**, 174 (2014).
- [26] M. Pica Ciamarra, E. Lippiello, C. Godano, and L. de Arcangelis, *Phys. Rev. Lett.* **104**, 238001 (2010).
- [27] H. Melosh, *Nature (London)* **379**, 601 (1996).
- [28] K. Felzer and E. Brodsky, *Nature (London)* **441**, 735 (2006).
- [29] M. Griffa, B. Ferdowsi, R. A. Guyer, E. G. Daub, P. A. Johnson, C. Marone, and J. Carmeliet, *Phys. Rev. E* **87**, 012205 (2013).
- [30] F. Giacco, L. Saggese, L. de Arcangelis, E. Lippiello, and M. Pica Ciamarra, *Phys. Rev. Lett.* **115**, 128001 (2015).
- [31] F. Giacco, L. de Arcangelis, M. P. Ciamarra, and E. Lippiello, *Phys. Rev. E* **97**, 010901(R) (2018).
- [32] J. Chatteraj, O. Gendelman, M. Pica Ciamarra, and I. Procaccia, *Phys. Rev. Lett.* **123**, 098003 (2019).
- [33] S. Henkes, M. van Hecke, and W. van Saarloos, *Europhys. Lett.* **90**, 14003 (2010).
- [34] S. H. Strogatz, *Nonlinear Dynamics and Chaos* (CRC Press, Boca Raton, FL, 2018).
- [35] S. Plimpton, *J. Comput. Phys.* **117**, 1 (1995).
- [36] P. A. Cundall and O. D. L. Strack, *Géotechnique* **29**, 47 (1979).
- [37] M. Urbakh, J. Klafter, D. Gourdon, and J. Israelachvili, *Nature (London)* **430**, 525 (2004).
- [38] O. M. Braun, I. Barel, and M. Urbakh, *Phys. Rev. Lett.* **103**, 194301 (2009).
- [39] J. Trømborg, J. Scheibert, D. S. Amundsen, K. Thøgersen, and A. Malthes-Sørensen, *Phys. Rev. Lett.* **107**, 074301 (2011).
- [40] E. E. Brodsky, V. Karakostas, and H. Kanamori, *Geophys. Res. Lett.* **27**, 2741 (2000).
- [41] E. E. Brodsky and N. J. van der Elst, *Annu. Rev. Earth Planet. Sci.* **42**, 317 (2014).